View metadata, citation and similar papers at core.ac.uk

brought to you by CORE

provided by White Rose Research Online

UNIVERSITY OF LEEDS

This is a repository copy of *Kinetics of the Reactions of Hydroxyl Radicals with Furan and its Alkylated Derivatives 2-Methyl Furan and 2,5-Dimethyl Furan*.

White Rose Research Online URL for this paper:
https://eprints.whiterose.ac.uk/164732/

Version: Accepted Version

Article:
Whelan, CA, Eble, J, Mir, ZS et al. (4 more authors) (2020) Kinetics of the Reactions of Hydroxyl Radicals with Furan and its Alkylated Derivatives 2-Methyl Furan and 2,5-Dimethyl Furan. The Journal of Physical Chemistry A. ISSN 1089-5639

https://doi.org/10.1021/acs.jpca.0c06321

© 2020 American Chemical Society. This is an author produced version of an article published in The Journal of Physical Chemistry A. Uploaded in accordance with the publisher's self-archiving policy.

Reuse
Items deposited in White Rose Research Online are protected by copyright, with all rights reserved unless indicated otherwise. They may be downloaded and/or printed for private study, or other acts as permitted by national copyright laws. The publisher or other rights holders may allow further reproduction and re-use of the full text version. This is indicated by the licence information on the White Rose Research Online record for the item.

Takedown
If you consider content in White Rose Research Online to be in breach of UK law, please notify us by emailing eprints@whiterose.ac.uk including the URL of the record and the reason for the withdrawal request.

eprints@whiterose.ac.uk
https://eprints.whiterose.ac.uk/

Kinetics of the Reactions of Hydroxyl Radicals with Furan and its Alkylated Derivatives 2-Methyl Furan and 2,5-Dimethyl Furan

Charlotte A. Whelan,[1] Julia Eble,[2] Zara S. Mir,[1] Mark A. Blitz,[1,3] Paul W. Seakins,[1] Matthias Olzmann,[2*] Daniel Stone[1*]

[1] School of Chemistry, University of Leeds, Leeds, LS2 9JT, UK

[2] Institute of Physical Chemistry, Karlsruhe Institute of Technology (KIT), Kaiserstr. 12, 76131 Karlsruhe, Germany

[3] National Centre for Atmospheric Science, School of Chemistry, University of Leeds, Leeds, LS2 9JT, UK

* Corresponding authors

Abstract

Furans are promising second generation biofuels with comparable energy densities to conventional fossil fuels. Combustion of furans is initiated and controlled to a large part by reactions with OH radicals, the kinetics of which are critical to understand the processes occurring under conditions relevant to low-temperature combustion. The reactions of OH radicals with furan (OH + F, R1), 2-methyl furan (OH + 2-MF, R2), and 2,5-dimethyl furan (OH + 2,5-DMF, R3) have been studied in this work over the temperature range 294 to 668 K at pressures between 5 mbar and 10 bar using laser flash photolysis coupled with laser-induced fluorescence (LIF) spectroscopy to generate and monitor OH radicals under pseudo-first-order conditions. Measurements at $p \leq 200$ mbar were made in N_2, using H_2O_2 or $(CH_3)_3COOH$ radical precursors, while those at $p \geq 2$ bar were made in He, using HNO_3 as the radical precursor. The kinetics of the reactions R1-R3 were observed to display a negative dependence on temperature over the range investigated, indicating the dominance of addition reactions under such conditions, with no significant dependence on pressure observed. Master equation calculations are in good agreement with the observed kinetics, and a combined parameterisation of addition channels and abstraction channels for R1-R3 is provided on the basis of this work and previous shock tube measurements at higher temperatures. This work significantly extends the temperature range previously investigated for R1 and represents the first temperature-

dependent measurements of R2 and R3 at temperatures relevant for atmospheric chemistry and low-temperature combustion.

Introduction

Furans are a class of aromatic cyclic ethers that have been proposed as potential biofuels owing to developments in their production from lignocellulosic waste biomass.[1-4] The unsubstituted furan (F) and its alkylated derivatives 2-methylfuran (2-MF) and 2,5-dimethylfuran (2,5-DMF), shown in Figure 1, are of particular interest for use as transport fuels, with 2,5-DMF showing notable promise owing to its similar energy density to gasoline and lower emissions of NO_x (NO_x = NO + NO_2), hydrocarbons and particulate matter compared to alternative alcohol-based biofuels.[5-10] These properties could be exploited further under low-temperature combustion conditions (T < 1000 K), with the production of furans from waste biomass also providing significant advantages over first generation biofuels, the production of which can come into competition with the growth of food crops. Furans are also released into the atmosphere as a result of biomass burning,[11-17] and are generated during the atmospheric oxidation of biogenic compounds such as isoprene and butadiene.[18, 19] The use of furans as biofuels could lead to substantial further emissions into the atmosphere, with potential impacts on air quality and climate.

The combustion and atmospheric oxidation of furans are primarily initiated by reaction with the OH radical. Assessment of the feasibility for use of furans as biofuels, and of any associated environmental impacts, thus requires knowledge of the kinetics for reactions of furans with OH under relevant conditions. Reactions of OH radicals with furan species can proceed via addition of OH to the furan ring, H atom abstraction from the ring, or, in the case of substituted furans, including 2-MF and 2,5-DMF, H atom abstraction from one of the substituent groups, with possible combinations leading to the potential for complex temperature- and pressure-dependent reaction kinetics.

The kinetics of OH + F (R1), 2-MF (R2), and 2,5-DMF (R3) have been the subject of studies at room temperature[20-24] and at temperatures above ~890 K,[25] but there has been only a single experimental investigation[26] of the temperature dependence of OH + F at temperatures relevant to low-temperature combustion and atmospheric oxidation, and there have been no measurements of the temperature dependence for OH + 2-MF or OH + 2,5-DMF kinetics under such conditions.

OH + F → products (R1)

OH + 2-MF → products (R2)

OH + 2,5-DMF → products (R3)

At temperatures between 890 and 1388 K and pressures between 1 and 2 bar, shock tube experiments by Elwardany *et al.*[25] have shown that the rate coefficients for R1-R3 increase with increasing temperature, with no significant dependence on pressure, indicating that abstraction channels dominate under these conditions. However, some curvature is evident in the Arrhenius plot for R1, with parameterisation of the rate coefficient for OH + F requiring a modified Arrhenius expression, suggesting the occurrence of multiple reaction channels. Flash photolysis experiments to investigate the kinetics of R1 at temperatures between 254 and 425 K in 40-200 mbar of Ar by Wine and Thompson[26] also showed no significant dependence on pressure, but with the temperature dependence demonstrating a decrease in the rate coefficient with increasing temperature and thus indicating the dominance of addition channels under conditions relevant to atmospheric oxidation.

The kinetics of OH + 2-MF and OH + 2.5-DMF have also been studied at room temperature,[22, 24] with rate coefficients generally observed to increase with increasing substitution of the furan ring. Although the temperature-dependent kinetics of R2 and R3 have not been studied experimentally in the regime relevant for atmospheric chemistry or low-temperature combustion, comparison of the room temperature measurements of k_2 and k_3 with those obtained in the shock tube experiments[25] at higher temperatures indicate addition channels play a key role at lower temperatures, with abstraction becomingly increasingly important as the temperature increases.

The competition between addition and abstraction channels has also been indicated by several studies in which theoretical approaches have been used to determine the potential energy surfaces and kinetics for reactions R1-R3.[27-32] Such approaches indicate that addition of OH to the C2/C5 position of the furan ring dominates under conditions relevant to low-temperature combustion for R1,[27-29] R2,[29-31] and R3,[29] owing to resonance stabilisation. The predicted kinetics[28, 29] for R1 are in good agreement with measurements at temperatures below 425 K. [21-23, 26] However, the predicted kinetics indicate that addition channels for R1 dominate at temperatures below 2000 K, in conflict with the observations by Elwardany *et al.*[25] which indicate that abstraction channels dominate at temperatures above 1000 K. For R2 and R3, the predicted kinetics[29, 31, 32] overestimate the observations made by Elwardany *et al.*,[25] although the predicted kinetics for R2[31] do reproduce the room temperature measurements.[22, 24]

Experimental determination of the kinetics for R1-R3 under conditions relevant for atmospheric chemistry and low-temperature combustion is thus essential to evaluate the potential development, use, and impacts of furan-based biofuels. In this work we report measurements of the kinetics of OH + F (R1), OH + 2-MF (R2), and OH + 2,5-DMF (R3) at temperatures between 294 K and 668 K and pressures ranging from 5 mbar to 10 bar. Experiments were performed using flash photolysis of gas mixtures containing an OH radical precursor and the furan under investigation under pseudo-first-

order conditions in N_2 or He bath gas, combined with laser-induced fluorescence (LIF) to monitor the behaviour of OH radicals in the system. In addition, master equation analysis (MESMER) was carried out on these reactions and the results were compared to the experimental rate coefficients. This provides further insight into these reaction, especially the temperature ranges where the reaction switches from addition to abstraction.

Experimental

Pressures ≤ 200 mbar

Experiments at pressures at and below 200 mbar were conducted at the University of Leeds, UK, in a slow flow reactor which has been described in detail in previous work.[33-35] Precursor gas mixtures were prepared in a glass gas manifold and passed into a stainless steel six-way cross at known flow rates determined by calibrated mass flow controllers. The pressure in the reaction cell was monitored by a capacitance manometer (MKS Instruments, 626A) and was controlled throttling the exit to the cell using a needle valve on the exhaust line leading to the pumps. Heating of the reaction cell was achieved by a series of cartridge heaters surrounding the cell, with temperatures monitored by K-type thermocouples situated close to the reaction zone.

The furan (F (Sigma-Aldrich, 99 %), 2-MF (Sigma-Aldrich, 99 %), or 2,5-DMF (Sigma-Aldrich, 99 %)) was purified by a series of freeze-pump-thaw cycles and prepared at a known concentration in N_2 and stored in a darkened glass bulb. Concentrations of the furan were such as to ensure pseudo-first-order conditions with respect to OH. Precursors to OH, *t*-butyl hydroperoxide ($(CH_3)_3COOH$) (Sigma-Aldrich, 70 % v/v aqueous) or hydrogen peroxide (H_2O_2) (Sigma-Aldrich, 50 % v/v aqueous) were degassed and entrained into the precursor gas flow using a known flow of N_2 carrier gas. N_2 (BOC, oxygen free, 99.99 %) and, where used, O_2 (BOC, 99.999 %) were used as supplied. Experiments were performed at each temperature over a range of pressures between 5 and 200 mbar, and concentrations of O_2 (up to 4.5×10^{16} cm^{-3}) to investigate any possible effects of OH recycling owing to peroxy radical chemistry. No evidence was observed for any influence of O_2 on the kinetics reported in this work. Precursor concentrations were typically varied in the ranges $10^{14} – 10^{15}$ cm^{-3} for H_2O_2 and $(CH_3)_3COOH$, and $10^{13} – 10^{15}$ cm^{-3} for the furan.

Chemistry in the cell was initiated by the pulsed laser photolysis of the peroxide OH precursor at λ = 248 nm using a KrF excimer laser (Lambda Physik Compex, typical fluence 10-30 mJ cm^{-2}) or λ = 266 nm using the 4th harmonic of an Nd:YAG laser (Continuum Powerlite 8010, typical fluence ~20 mJ cm^{-2}). At temperatures below 500 K, experiments were performed with either H_2O_2 or

$(CH_3)_3COOH$ used as the OH precursor, with experiments at temperatures above 500 K performed using H_2O_2 as the OH precursor owing to the decomposition of $(CH_3)_3COOH$ on the walls of the reactor at the higher temperatures. No significant differences in results were observed for experiments using different OH radical precursors or different photolysis sources under otherwise identical conditions. Experiments were typically performed at a pulse repetition frequency of 10 Hz, although the lasers were also operated at lower repetition rates to ensure that there were no interferences from photolysis of reaction products.

The temporal behaviour of OH radicals in the system was monitored by off-resonance laser-induced fluorescence (LIF) following excitation of the $A^2\Sigma$ (v'=1) ← $X^2\Pi$ (v''=0) $Q_1(1)$ transition at 282 nm generated using the 532 nm output of an Nd:YAG (Continuum Powerlite 8010) to pump a dye laser (Spectra Physics PDL-3) operating on Rhodamine-6-G dye. The off-resonant OH fluorescence at ~308 nm was passed through an interference filter (Barr Associates, 308 ± 5 nm) and detected by a photomultiplier (Electron tube 9813 QB) mounted perpendicular to the plane of the photolysis and probe laser beams. The photomultiplier signal was digitised, integrated by an oscilloscope (LeCroy LT262), and passed to a computer for data analysis. The time delay between the photolysis and probe lasers was controlled by a homebuilt digital delay generator based on National Instruments hardware and was varied to enable monitoring of the OH profiles as a function of time following photolysis of the gas mixture. Kinetic traces typically consisted of 200 time points, with each time point averaged 5-10 times.

Pressures ≥ 2 bar

Measurements at pressures at and above 2 bar were performed at the Karlsruhe Institute of Technology (KIT), Germany, in a slow flow reactor which has also been described in detail in previous work.[36, 37] While there are similarities to the experimental technique described above, there are some key differences which warrant further description.

Precursor gases, consisting of the OH precursor nitric acid (HNO_3) and the furan of interest in He bath gas, were mixed in a capillary and passed into a stainless steel reaction cell at known flow rates controlled by calibrated mass flow controllers. The pressure in the cell was regulated with a pressure controller mounted in the exhaust line of the cell, with a pressure transducer connected to the inlet line used to ensure there were no significant pressure gradients across the cell. The cell was heated by resistance wires around the cell, with the precursor gases preheated by a heating cord surrounding the inlet capillary prior to its entry into the cell. The temperature in the cell was measured by thermocouples situated at the inlet and outlet to the cell, with the typical temperature difference

between the two thermocouples typically ~1 K and never exceeding 5 K, and the mean value taken as the reaction temperature.

Gas mixtures of HNO_3 in He and the furan in He were prepared in gas cylinders and stored for at least 12 h before use to ensure complete mixing. To minimise the extent of decomposition of HNO_3 in the cylinder, HNO_3 was always freshly produced before preparation of a mixture by adding concentrated H_2SO_4 (98 %, Roth) dropwise to ice-cooled solid KNO_3 (≥ 99 %, Roth), and mixtures were used for a maximum of 4 days. There was no observed dependence of the measured kinetics on the fill level or the age of the gas mixtures. Peroxide precursors to OH were also tested at KIT but were found less suitable for the high pressure experiments, probably owing to unavoidable trace concentrations of O_2 and H_2O which would cause significant quenching of OH LIF signals at such high pressures. The signal-to-noise ratios were consistently worse using peroxide precursors compared to those using HNO_3. It can also be noted that HNO_3 has a substantially higher vapour pressure than the peroxide precursors, which facilitates gas mixture preparation for the high pressure experiments. Concentrations of species in the gas mixtures were varied in the ranges $(0.46 – 4.97) \times 10^{16}$ cm^{-3} for HNO_3, $(0.11 – 9.01) \times 10^{15}$ cm^{-3} for furan (Sigma Aldrich, ≥ 99 %), $(0.06 – 11.8) \times 10^{15}$ cm^{-3} for 2-methyl furan (Sigma Aldrich, 99 %), and $(0.06 – 4.37) \times 10^{15}$ cm^{-3} for 2,5-dimethyl furan (Sigma Aldrich, 99 %), with gas mixtures prepared to ensure that OH radicals produced on photolysis were under pseudo-first-order conditions. Experiments were performed at each temperature at total pressures of 2, 5 and 10 bar.

Photolysis of gas mixtures was achieved at a wavelength of 248 nm using a KrF excimer laser (Lambda Physik Compex102, typical fluence 5-15 mJ cm^{-2}) with the pulse repetition frequency varied between 2 and 10 Hz and most experiments performed at a repetition frequency of 10 Hz. OH fluorescence was excited at 282 nm using the frequency-doubled output from a 308 nm XeCl excimer (Lambda Physik Compex102) pumped dye laser (Lambda Physik, ScanMate 2E) operating on Coumarin 153. Fluorescence photons at ~308 nm were detected by a photomultiplier tube (PMT, Hamamatsu, R22A) perpendicular to the photolysis and probe beams, with detection of scattered laser light minimised using a monochromator set to (308 ± 4) nm. The time delay between the photolysis and probe lasers was controlled by a delay generator (Stanford, DG535), and was varied as described above to give the OH profile as a function of time throughout the reaction of interest. OH profiles typically consisted of ninety time points which were each averaged ten times.

Results

Figure 2 shows typical OH profiles recorded during experiments at the University of Leeds and at KIT. Pseudo-first-order rate coefficients describing the loss of OH under given conditions were determined by fitting to the OH profiles, and the bimolecular rate coefficients for a given temperature and pressure determined from the slopes of the bimolecular plots of the pseudo-first-order rate coefficients plotted against the concentration of the furan under investigation. Typical bimolecular plots are shown in Figure 3.

OH + furan

Figure 4 shows the temperature dependence of the bimolecular rate coefficient for OH + F (k_1) determined by experiments in Leeds and at KIT. A summary of results is given in Table 1. No significant dependence on pressure was observed for k_1 under the conditions investigated. At 298 K, results from Leeds give $k_1 = (3.34 \pm 0.48) \times 10^{-11}$ cm^3 s^{-1}, with those determined at 294 K at KIT giving $k_1 = (3.45 \pm 0.13) \times 10^{-11}$ cm^3 s^{-1}. Uncertainties are reported as 2σ.

Previous flash photolysis experiments at 298 K gave a rate coefficient for R1 of $(4.0 \pm 0.3) \times 10^{-11}$ cm^3 s^{-1},[26] with similar results obtained in relative rate experiments at pressures between 980 and 1013 mbar of air at room temperature using a range of reference compounds including *n*-hexane (giving $k_1 = (4.01 \pm 0.30) \times 10^{-11}$ cm^3 s^{-1}),[21] isoprene (giving $k_1 = (3.98 \pm 0.35) \times 10^{-11}$ cm^3 s^{-1}),[23] and propene (giving $k_1 = (4.19 \pm 0.21) \times 10^{-11}$ cm^3 s^{-1}).[22] However, results obtained from a discharge flow experiment at 295 K in 2.7 mbar of He gave a significantly higher value of $k_1 = (1.05 \pm 0.08) \times 10^{-10}$ cm^3 s^{-1}, but this study also reported kinetics for the reaction between OH radicals and thiophene that were systematically higher than other results reported in the literature.[20]

While the results obtained in this work at 298 K are lower than previous determinations, they are within the uncertainties reported by Wine and Thompson[26] and Tuazon *et al.*[23] The higher rate coefficients observed in previous work may result from the OH generation methods used in previous studies which could give rise to the possibility for secondary chemistry. In the flash photolysis study by Wine and Thompson,[26] OH radicals were produced by the photolysis of water vapour at wavelengths between 165 nm and 185 nm, leading to the production of H atoms in equal amounts to OH. Although experiments were performed in which the flash intensity was varied by a factor of ~4-5 to rule out the possibility of furan photolysis, the chemistry of the H atoms in the system may have affected the observed kinetics. In the relative rate studies, continuous UV lamp photolysis of methyl nitrite was used to generate OH, with photolysis wavelengths of > 290 nm,[23] 320-480 nm[22] and 350-

400 nm.[21] This method also leads to the production of other reactive species, including CH_3O, HO_2, NO and NO_2,[21] which may have had some small effects on the observed kinetics. For one of the relative rate studies,[22] which used propene as the reference compound and reported $k_1 = (4.19 \pm 0.21) \times 10^{-11}$ cm^3 s^{-1}, the authors did note significant scatter in their data and negative intercepts in the plots showing the change in furan concentration against the change in concentration of the reference compound used to determine k_1. The use of current recommendations[38] for the reference compound kinetics in the relative rate studies[21-23] would lead to changes in k_1 of < 5 %.

The temperature dependence observed for k_1 indicates the dominance of addition channels over the temperature range investigated, in agreement with the work of Wine and Thompson[26] and the general behaviour observed for OH + alkene and OH + aromatic reactions over similar temperature ranges,[38] and suggests the formation of an OH-F adduct in a barrierless reaction as predicted by theory.[27-29] At the higher temperatures (924-1388 K for R1) investigated by Elwardany *et al.*,[25] a positive temperature dependence was observed, indicating the importance of activated abstraction channels at such temperatures. A full parameterisation of the results obtained in this work combined with those of Eldwardany *et al*. is given by the master equation analysis discussed below and is shown in Figure 4.

OH + 2-methyl furan

Rate coefficients for OH + 2-MF (k_2) are also shown in Figure 4 as a function of temperature and summarised in Table 2. The general behaviour of k_2 as a function of temperature is similar to that for k_1, with no significant dependence on pressure over the ranges investigated, although k_2 is typically higher than k_1 for a given temperature. At 298 K, results from experiments in this work at $p \leq 200$ mbar gave $k_2 = (7.34 \pm 0.29) \times 10^{-11}$ cm^3 s^{-1} and those from experiments at $p \geq 2$ bar at 296 K gave $k_2 = (6.80 \pm 0.30) \times 10^{-11}$ cm^3 s^{-1}. Previous investigations of OH + 2-MF at room temperature gave $k_2 = (6.19 \pm 0.21) \times 10^{-11}$ cm^3 s^{-1} and $k_2 = (7.31 \pm 0.35) \times 10^{-11}$ cm^3 s^{-1} from relative rate experiments using propene and 1,3,5-trimethylbenzene used as reference compounds, respectively.[22, 24] Relative rate experiments at 1013 mbar using propene and *trans*-2-butene as reference compounds for OH + 2-MF and OH + 2,5-DMF, respectively, gave rate coefficients $k_2 = (6.19 \pm 0.21) \times 10^{-11}$ cm^3 s^{-1} and $k_3 = (1.32 \pm 0.09) \times 10^{-10}$ cm^3 s^{-1},[22] with another study at 980 mbar using 1,3,5-trimethylbenzene as the reference compound giving $k_2 = (7.31 \pm 0.35) \times 10^{-11}$ cm^3 s^{-1}.[24] Similarly to the relative rate determination of k_1 using propene as the reference compound, the plot of the change in 2-MF concentration against the change in propene concentration used to determine k_2 displayed significant

scatter and a significant non-zero intercept which may have impacted the determination of k_2 in the previous work.[22]

The results obtained in this work indicate a more significant temperature dependence than observed for k_1 but with similar implications regarding the importance of barrierless addition channels over the temperature range investigated. Similarly to R1, results obtained in the shock tube study by Elwardany *et al*.[25] demonstrate the importance of abstraction channels in R2 at higher temperatures than those investigated in this work. A full parameterisation of k_2 based on the results obtained in this work combined with those of Eldwardany *et al*. is described below.

OH + 2,5-dimethyl furan

Experiments at $p \leq 200$ mbar gave an average value of $k_3 = (1.15 \pm 0.07) \times 10^{-10}$ cm^3 s^{-1} at 298 K while those at $p \geq 2$ bar at 294 K gave $k_3 = (0.92 \pm 0.04) \times 10^{-10}$ cm^3 s^{-1} (as shown in Figure 4 and Table 3), with results at these temperatures indicating no significant dependence on pressure. Previous studies of k_3 at room temperature gave values of $(1.32 \pm 0.10) \times 10^{-10}$ cm^3 s^{-1} and $(1.25 \pm 0.04) \times 10^{-10}$ cm^3 s^{-1} using the relative rate technique at 1013 mbar with *trans*-2-butene as the reference compound[22] and at 980 mbar with 1,3,5-trimethylbenzene as the reference compound,[24] respectively.

At higher temperatures there was no significant dependence of k_3 on pressure, although there was evidence for OH production following the photolysis of 2,5-DMF in the absence of any OH precursor at temperatures above 410 K and pressures below 67 mbar. The results given for k_3 at $p \leq 200$ mbar are reported as the mean of those obtained in experiments where results were unaffected by photolysis of 2,5-DMF. For all temperatures investigated at $p \geq 2$ bar, there was no evidence for pressure dependence of k_3.

Results obtained in this work are summarised in Table 3 and Figure 4. Figure 4 also shows the results of Elwardany *et al*.[25] at pressures between 1 and 2 bar and temperatures in the range 915-1278 K. A combined fit to the data obtained in this work with that of Elwardany *et al*., based on the master equation analysis described below, is also provided in Figure 4. For a given temperature, k_3 is greater than k_2, which is greater than k_1, owing to increased stabilisation of the OH-furan adduct with increased substitution of the furan ring from F to 2-MF to 2,5-DMF, which is discussed in detail below.

Master Equation Calculations

Master equation calculations were performed for reactions R1-R3 using the Master Equation Solver for Multi-Energy well Reactions (MESMER),[39] in order to rationalise the observed kinetics for R1-R3 from a more fundamental perspective. MESMER has been described in detail in previous work,[33, 35, 39] and uses an energy grained master equation in which the rovibrational energy states for reactants, transition states, intermediates, and products, are partitioned into a number of grains which contain a defined number of states. The energy grains representing initial reactants are assigned populations by invoking a Boltzmann distribution, with those representing other species set to a population of zero. Changes in the population distribution among grains can occur through collisional energy transfer via interactions with a thermal bath gas, or through reactions controlled by the microcanonical rate coefficients in the system which involve the transformation of one species to another. Reactive processes within the system are described by RRKM theory for activated reactions and inverse Laplace transformations (ILT) applied to barrierless reactions. Collisional energy transfer is described by an exponential down model in which the average energy transferred between grains on collision is described by the parameter $<\Delta E>_{down}$.

MESMER has been used by Yuan *et al*.[29] to study reactions R1-R3 and the subsequent reactions of the OH-addition products with O_2 under atmospheric conditions using potential energy surfaces determined at the RHF-UCCSD(T)-F12a/cc-pVDZ-F12 level of theory. Under such conditions, Yuan *et al*. demonstrated that the reactions of OH with furans proceed via formation of a van der Waals complex and are dominated by addition of OH to the C atom adjacent to the O atom (i.e. in the C2/C5 position for F, 2-MF and 2,5-DMF), forming a chemically activated OH-adduct, which can undergo collisional deactivation or a ring-opening reaction to form a number of resonance stabilised *E/Z* conformers that are able to interconvert. In air, addition of O_2 to the OH-adduct is expected to dominate over the ring-opening reactions, forming peroxy radicals which are ultimately expected to produce furanones, epoxides, and dicarbonyl compounds which have been observed in previous chamber studies.[40]

Figure 5 shows a simplified potential energy surface for the initial steps in the addition reactions of OH with furans in the absence of O_2 (full details of the potential energy surfaces are given in the Supporting Information).[29] In this work, we have used the MESMER input files developed by Yuan *et al*.[29] for reactions R1-R3 to investigate the kinetics of these reactions over the experimental temperature and pressure ranges reported in this work and in the previous shock tube study, with minor reaction channels involving addition at the C3 and C4 positions omitted and subsequent isomerisation reactions of the products shown in Figure 5 excluded to improve computational efficiency. For OH + 2-MF, addition at the C2 and C5 positions were considered, requiring exclusion

of channels involving species R2B_Z2, R5B_Z2, R2B_E1, R5B_E1, R2B_E2, and R5B_E2 to improve computational efficiency owing to the complexity of this C2 and C5 potential energy surface. Simulations using the full potential energy surfaces described by Yuan *et al*. and those with the minor modifications indicated that such modifications reduce the computational cost of the fits, without any significant loss in accuracy. Collisional energy transfer was modelled using $\langle\Delta E\rangle_{down} = 250 \times (T/298)^{0.25}$ cm^{-1} for N_2,[29, 41-43] $180 \times (T/298)^{0.5}$ cm^{-1} for Ar,[41, 43] and 125 cm^{-1} $\times (T/298)^{1.0}$ for He.[41, 43] The initial reaction between OH and the furan occurs on barrierless surfaces to form pre-reaction complexes (see Figures 5 and S1). Inverse Laplace Transform of the macroscopic rate coefficient, $k = A\ T^n$, for these reactions were used to generate the microcannocial rate coefficients, $k(E)$, required for the Master Equation calculation. The other microcannonical rate coefficients, where the reaction is described by a defined transition-state, were calculated using RRKM theory. Direct OH abstraction from the furan is a bimolecular process and, as such, is not formally part of the master equation as there are no microcannonical rate coefficients associated with it. However, it is represented in MESMER as an irreversible loss from the system via *A* and *Ea* parameters.

The MESMER predictions were compared to the measured rate coefficients and the difference was minimized through data fitting using a Levenburg-Marquardt algorithm, where the fit parameters were the ILT parameters describing the initial formation of the van der Waals complex in the addition channels, the transition state energy leading to the OH-addition product (TS2), and the Arrhenius parameters describing the abstraction channels. A pure harmonic vibration only model is used for the MESMER description of each reaction. This framework is flexible enough so that a good fit to the experimental data should be achievable. However, the adjustment of the transition-states energy parameters may not coincide with the theoretical *ab initio* energies due to the imposition of this harmonic vibration only model. This perturbation is especially significant for the low frequency modes, which can show significant anharmonicity. This can be particularly important where the low frequency modes are hindered rotors, in OH + isoprene, for example, the energy of the addition adduct varied significantly between a model using harmonic frequencies and a model using hindered rotors to describe the low frequency modes.[43] However, for cyclic systems such as those involving furans the impact of hindered rotors is less than for OH + alkenes and therefore a pure harmonic model for vibrations should not significantly impact the results. The fit energies for the transition state leading to the OH-addition product (TS2) discussed below may be, in part, a consequence of the treatment of the low frequency modes, but the differences between the calculated and fit energies are not outside the accuracy of the calculations.

Initial simulations with MESMER indicated dissociation of the initial OH-furan adduct at temperatures above 800 K, with equilibrium behaviour expected as shown by the simulated concentration time-profiles for the furan, OH, and the OH-furan adduct for reactions R1-R3 (see Supporting Information for further details). The effective rate coefficient for dissociation of the OH-furan adduct is ~10,000 s^{-1} at ~900 K for furan and 2-methyl furan and ~10,000 s^{-1} at ~1100 K for 2,5-dimethyl furan. The flash photolysis experiments reported in this work were conducted at temperatures at which there is no significant dissociation of the OH-furan adduct, and thus the observed OH profiles represent simple OH loss and can be fully modelled in MESMER to provide a good fit. However, it is likely that the shock tube data were affected by equilibrium behaviour, although this was not evident in the analysis by Elwardany et al. In our attempts to fit the data reported in this work with the shock tube data of Elwardany et al., it was observed that there was a systematic problem fitting the shock tube data. This was most evident in the OH + 2-MF data, where the fit result was too high at temperatures below 1000 K and too low at temperatures above 1200 K (see Supporting Information), and was evident for all of R1-R3. We suggest this problem might result from not recognising the equilibrium behaviour in the shock tube data, leading to the reported rate coefficients being perturbed. To overcome this problem we have omitted all the shock tube data in the range 800-1100 K, above which range abstraction will dominate.

The results of the MESMER analysis are given in Table 4 and are shown in Figure 4. From Figure 4 it can be seen that the fits to the data are good, and the systematic problem of fitting the shock tube data is almost absent. In general, the fits require a reduction in the energy of the transition state leading from the van der Waals complex to the initial adduct compared to the calculated energy, but this reduction was not more 6 kJ mol^{-1}, which is within the uncertainties of the calculations and the TS2 fit uncertainties. For OH + F, the fits require the energy of the transition state to be reduced from the calculated value of -10.1 kJ mol^{-1} to –(13.9 ± 4.0) kJ mol^{-1}, with the ILT parameters describing the initial formation of the van der Waals complex given by (7.4 ± 8.2) × 10^{-11} (T/298 K)$^{-(1.11 \pm 0.34)}$ cm^3 s^{-1} and the abstraction channel described by (2.0 ± 2.8) × 10^{-10} exp(-(34.7 ± 16.5) kJ mol^{-1}/RT) cm^3 s^{-1} (errors are 2σ). The ILT parameters determined in MESMER describe the initial formation of the van der Waals complex, but do not represent the overall rate coefficient for the addition channel, for which a fit to the Troe formalism is given below. Previous calculations[28] of the potential energy surface for abstraction channels in OH + F indicated a significantly higher barrier to reaction of 62.9 kJ mol^{-1} for the lowest energy abstraction pathway than indicated in this work, but such a barrier implies that abstraction channels are not important at temperatures below 2000 K and results in significant underprediction of the results of Elwardany *et al.*[25] For OH + 2-MF, the transition state energy for production of the adduct from the van der Waals complex was lowered from the calculated

energy of -16.2 kJ mol^{-1} to -(22.0 ± 13.5) kJ mol^{-1}, and that for OH + 2,5-DMF was lowered from -21.4 kJ mol^{-1} to -(26.4 ± 9.1) kJ mol^{-1}. The MESMER fits indicate that the formation of the van der Waals complexes for OH + 2-MF and OH + 2,5-DMF, from which the addition channels proceed, can be described by the ILT parameters (10.9 ± 2.0) × 10^{-11} (*T*/298 K)$^{-(1.29 \pm 2.72)}$ cm^3 s^{-1} and (10.7 ± 0.35) × 10^{-11} (*T*/298 K)$^{-(1.29 \pm 1.02)}$ cm^3 s^{-1}, respectively, and that the abstraction channels can be described by (4.2 ± 4.9) × 10^{-10} exp(-(31.6 ± 13.2) kJ mol^{-1}/*RT*) cm^3 s^{-1} and (1.1 ± 0.9) × 10^{-10} exp(-(16.3 ± 7.2) kJ mol^{-1}/*RT*) cm^3 s^{-1}. Previous calculations for the barrier to abstraction for OH + 2-MF gave values of 13.1 kJ mol^{-1} [30] and 22.6 kJ mol^{-1},[31] in broad agreement with the results obtained in this work, and is lower than that for OH + F owing to the relative ease of abstraction from the methyl group and subsequent formation of allylic systems compared to abstraction from the ring. Similarly, the barrier to abstraction for OH 2,5-DMF is lower than that for OH + F, and close to that for OH + 2-MF, with the result obtained in this work for OH + 2,5-DMF in agreement with the value of 15.5 kJ mol^{-1} calculated in previous work.[32] However, it is noted that omitting the shock tube data in the temperature range 800 – 1100 K leads to large errors in the abstraction barriers, especially for 2-MF.

The MESMER simulations are in agreement with the observed kinetics, but do indicate a weak pressure dependence in the kinetics of the addition channels for R1-R3, which increases in significance with increasing temperature, with some dissociation of the OH-adducts back to reactants at temperatures above 800 K. These effects are more significant for OH + F than for OH + 2-MF or OH + 2,5-DMF, partially owing to the increased density of states for OH + 2-MF and OH + 2,5-DMF compared to OH + F. However, the predicted pressure dependence of the addition channels is of minor importance in the overall reaction since the abstraction channels become increasingly important at the temperatures at which the pressure dependence of the addition channels is significant. The pressure dependence of the addition channels thus has minimal effects on the overall kinetics over the temperature and pressure ranges investigated in this work, as demonstrated in Figure 4 (further details are shown in Figure S6 in the Supporting Information). The lack of significant pressure dependence in the kinetics of R1-R3 predicted by MESMER over the temperature and pressure ranges investigated in this work is a consequence of the deep energy well for the one of the conformers (labelled R2B_Z3 in Figure 5) formed following the ring-opening reactions, which, coupled with the entropic cost of reformation of the ring system, makes this conformer an effective sink. The conformer R2B_Z3 is 179.9 kJ mol^{-1} lower than the entrance channel for R1, 185.1 kJ mol^{-1} lower for R2, and 191.6 kJ mol^{-1} lower for R3.[29] A deep energy well for R2B_Z3 tends to reduce the impacts of pressure on the kinetics for R1-R3, and the lack of observed pressure dependence for R1-R3 over the experimental conditions investigated is consistent with a deep energy well for R2B_Z3. The well depth for R2B_Z3 also explains the lack of observed pressure dependence for the

furan systems compared to OH-addition reactions involving alkenes and aromatic hydrocarbons, which typically do exhibit pressure dependence under similar conditions owing to the formation of addition products with well depths that are not as deep as those demonstrated for furans.

Figure 4 shows the MESMER fit to the data. The MESMER fits can be described by $k_1 = 3.5 \times 10^{-11} (T/300)^{-1.61} + 9.5 \times 10^{-11} (T/1000)^{-0.44} \exp(-(25.6 \text{ kJ mol}^{-1})/RT)$ cm^3 s^{-1}, $k_2 = 7.3 \times 10^{-11} (T/300)^{-1.97} + 5.3 \times 10^{-8} (T/1000)^{-4.19} \exp(-(72.8 \text{ kJ mol}^{-1})/RT)$ cm^3 s^{-1}, and $k_3 = 9.2 \times 10^{-11} (T/300)^{-1.78} + 2.0 \times 10^{-8} (T/1000)^{-4.15} \exp(-(60.3 \text{ kJ mol}^{-1})/RT)$ cm^3 s^{-1}, to describe the overall kinetics under the conditions relevant to this work. In order to provide a full parameterisation of the kinetics of the addition channels for R1-R3, which do exhibit some pressure dependence but is only significantly evident at higher temperatures than investigated in this work (Figure S6). MESMER simulations were performed using the fit parameters determined in this work over a wide range of number densities (10^{16}-10^{21} cm^{-3}) and temperatures (300-1300 K). The forward rate coefficients (k_f) describing the addition channels OH + furan → OH-adduct (corresponding to the addition components to k_1, k_2, and k_3) were described by the Troe formalism:

$$k_f(T,[\text{M}]) = \frac{k_0(T)[\text{M}]}{1+\frac{k_0(T)[\text{M}]}{k_\infty(T)}} F(x) \qquad \text{(E1)}$$

where $k_0(T)$ and $k_\infty(T)$ represent the low- and high-pressure limiting rate coefficients, respectively, and are given by the relationships $k_0(T) = A_0 (T / 298 \text{ K})^n$ cm^6 s^{-1} and $k_\infty(T) = A_\infty (T/298 \text{ K})^m$ cm^3 s^{-1}, [M] is the number density, and $F(x)$ is the collision broadening factor, which is given by the formulation described by Troe and Ushakov[44]:

$$F(x) = (1+\frac{x}{x_0})/[1+(\frac{x}{x_0})^{n_1}]^{1/n_1} \qquad \text{(E2)}$$

$$x = k_0(T)[\text{M}] / k_\infty(T) \qquad \text{(E3)}$$

$$n_1 = \left[\frac{\ln 2}{\ln(\frac{2}{F_{\text{cent}}})}\right] [1-b+b\,(\frac{x}{x_0})^q] \qquad \text{(E4)}$$

$$q = (F_{\text{cent}}-1)/\ln(\frac{F_{\text{cent}}}{10}) \qquad \text{(E5)}$$

The reverse rate coefficients (k_r) describing OH-adduct → OH + furan (corresponding to k_{-1}, k_{-2}, and k_{-3}) were included for simulations at $T \geq 800$ K and were linked to the kinetics of the corresponding forward reactions through the thermodynamic parameters $\Delta H^\ominus$ and $\Delta S^\ominus$ describing the equilibria between the forward (k_f) and reverse processes (k_r) over the simulated temperature range:[43]

$$k_r(T,[\text{M}]) = \frac{k_f(T,[\text{M}])}{RT} \times \exp\left(\frac{\Delta H^\circ}{RT}\right) \times \exp\left(-\frac{\Delta S^\circ}{R}\right) \qquad \text{(E6)}$$

Identification of the reverse rate coefficients was achieved via inspection of the eigenvalues in each system since the presence of multiple wells makes the system too complex to identify the contributions of individual rate coefficients. The second smallest eigenvalue, λ_2, in each system contains reverse rate coefficient data, but it refers to different well reactions as the temperature is increased (see Supporting Information for further details). At the highest temperatures, the reverse rate coefficient refers to OH formation and thus to equilibrium behaviour. For OH + F, reverse rate coefficients could only be determined for data above 1000 K (see Supporting Information for further details). Care was taken for each furan to ensure that only data referring to dissociation of the initial OH-addition product were included in the Troe analysis. For OH + F, data at $T \geq 1000$ K were included in the analysis, while analysis for 2-MF data included data at $T \geq 600$ K and that for OH + 2,5-DMF included data at $T \geq 1100$ K. For each reaction system, global fits to the MESMER outputs were performed to determine the parameters A_0, n, A_∞, m, x_0, b, F_{cent}, $\Delta H^\ominus$, and $\Delta S^\ominus$ in Equations 1-6. In this analysis each rate coefficient was assigned a 10 % error, and it was checked that the reduced χ^2 was equal or unity, or lower, in each fit, i.e. these expressions are, on average, within 10 % of the MESMER result.

The MESMER input files, outputs, and fits are shown in the Supporting Information. Figure 4 shows the Troe fit to the data, where this Troe fit is equal to the sum of the Troe expression describing the forward rate coefficient for the addition channel (parameters in Table 5) and the rate coefficient for the abstraction channel (parameters in Table 4). In general, this Troe fit is not flexible enough to fully describe the MESMER values, and it can be seen in Figure 4 that the rate coefficients at 300 K are underpredicted. However, it is noted that this Troe expression is within 10 % of the MESMER values.

Conclusions

The kinetics of R1-R3 have been studied over a wide range of temperatures (294-668 K) and pressures (5 mbar to 10 bar) relevant for atmospheric chemistry and low temperature combustion. Results indicate that addition of OH to the furan ring dominates the kinetics for the experimental conditions investigated, with abstraction channels becoming increasingly important at temperatures above ~900 K. However, results obtained in MESMER indicate that the OH-addition channels exhibit equilibrium behaviour in the temperature range 800-1200 K, which was not considered in the previous analysis of the shock tube data obtained in previous work. Troe expressions are provided to describe the rate coefficients for the addition channels.

No significant pressure dependence of the overall kinetics for R1-R3 was observed, with master equation calculations supporting these observations but indicating more significant effects of pressure on the addition channels at higher temperatures. The master equation calculations indicate that the lack of observed pressure dependence under the conditions investigated is a result of deep energy wells (> ~ -180 kJ mol^{-1}) in the potential energy surface following addition of OH to the furan ring and subsequent isomerisation of the addition adduct.

Supporting Information

This material is available free of charge *via* the Internet at http://pubs.acs.org. The Supporting Information contains details of the potential energy surfaces used in the MESMER analysis, structures of species in the MESMER simulations, details regarding the identification of equilibrium behaviour, MESMER output and Troe fits for the addition rate coefficients and reverse rate coefficients for R1-R3, and the MESMER input files.

Author Information

Corresponding Authors

Daniel Stone, d.stone@leeds.ac.uk, +44 113 343 6508

Matthias Olzmann, matthias.olzmann@kit.edu, +49 721 608 42918

Notes

The authors declare no competing financial interest.

Acknowledgements

We would like to thank Dr Liming Wang (School of Chemistry & Chemical Engineering, South China University of Technology, Guangzhou) for providing the MESMER input files used in the work reported by Yuan *et al.*[29] for use in this work. CAW thanks the Engineering and Physical Sciences Research Council for a studentship. The authors are also grateful to the Natural Environment Research Council (NERC, grant reference NE/L010798/1) for funding. Work at KIT was supported by the Deutsche Forschungsgemeinschaft (DFG, German Research Foundation) – Projektnummer 237267381 – TRR 150.

Tables

	T / K	k_1 / 10^{-11} cm^3 s^{-1}
$p \leq 200$ mbar	298	3.34 ± 0.48
	340	2.97 ± 0.23
	380	2.54 ± 0.20
	420	2.40 ± 0.06
	460	1.62 ± 0.21
	500	2.03 ± 0.05
	548	1.47 ± 0.12
	595	1.27 ± 0.11
$p \geq 2$ bar	294	3.45 ± 0.13
	307	3.36 ± 0.12
	322	3.22 ± 0.11
	341	2.92 ± 0.09
	358	2.7 ± 0.08
	382	2.62 ± 0.10
	407	2.29 ± 0.07
	435	2.14 ± 0.12
	453	2.00 ± 0.08
	493	1.70 ± 0.08
	518	1.52 ± 0.10
	560	1.24 ± 0.07

Table 1: Summary of results for k_1 as a function of temperature.

	T / K	k_2 / 10^{-11} cm^3 s^{-1}
$p \leq 200$ mbar	298	7.34 ± 0.29
	340	6.12 ± 0.25
	380	5.17 ± 0.30
	420	4.60 ± 0.20
	460	3.95 ± 0.12
	500	3.75 ± 0.36
	580	1.99 ± 0.05
	668	1.56 ± 0.11
$p \geq 2$ bar	296	6.80 ± 0.30
	308	6.60 ± 0.30
	322	6.40 ± 0.30
	341	5.50 ± 0.20
	357	5.00 ± 0.20
	378	4.60 ± 0.20
	406	3.98 ± 0.19
	431	3.55 ± 0.15
	453	3.37 ± 0.14
	490	2.68 ± 0.10
	520	2.35 ± 0.13
	566	1.60 ± 0.07

Table 2: Summary of results for k_2 as a function of temperature.

	T / K	k_3 / 10^{-11} cm^3 s^{-1}
$p \leq 200$ mbar	298	11.50 ± 0.70
	410	6.20 ± 0.70
	475	4.60 ± 0.50
	535	3.40 ± 0.40
	550	3.50 ± 0.50
	610	3.10 ± 0.50
	635	2.90 ± 0.50
$p \geq 2$ bar	295	9.20 ± 0.40
	307	10.10 ± 0.50
	321	7.80 ± 0.40
	337	6.50 ± 0.30
	358	5.70 ± 0.20
	380	5.40 ± 0.20
	407	4.60 ± 0.20
	435	4.06 ± 0.13
	455	3.60 ± 0.13
	491	3.86 ± 0.19
	519	3.44 ± 0.18
	557	2.85 ± 0.14

Table 3: Summary of results for k_3 as a function of temperature.

Reaction	A_{vdw} / 10^{-11} cm^3 s^{-1}	n	TS_R2 ZPE / kJ mol^{-1}	$A_{abstraction}$ / 10^{-10} cm^3 s^{-1}	$E_{a,abstraction}$ / kJ mol^{-1}	χ^2 per point
OH + F	7.4 ± 8.2	-1.11 ± 0.33	-13.9 ± 4.0	1.9 ± 2.8	34.7 ± 16.5	0.85
OH + 2-MF	10.8 ± 2.00	-1.29 ± 2.73	-22.0 ± 13.5	4.2 ± 4.9	31.6 ± 13.2	1.21
OH + 2,5-DMF	10.7 ± 0.35	-1.29± 1.03	-26.4 ± 9.1	1.1 ± 0.9	16.3 ± 7.2	1.95

Table 4: Summary of fit parameters obtained in MESMER to describe the kinetics of R1-R3 by fitting to experimental data reported in this work and by Elwardany *et al.*[25] A_{vdw} and $A_{abstraction}$ represent the pre-exponential factors for the formation of the van der Waals complex and for the abstraction channel, respectively, n represents the exponent to which the (T/298 K) term is raised in the ILT parameters describing the formation of the van der Waals complex, TS_R2 ZPE is the zero-point-corrected energy for the transition state leading from the van der Waals complex to the addition product (as shown in Figure 5), and $E_{a,abstraction}$ is the activation energy for the abstraction channel. Uncertainties are 2σ. The overall rate coefficient for R1, R2, or R3 for a given pressure and temperature is given by the sum of the abstraction rate coefficient, described by the Arrhenius parameters $A_{abstraction}$ and $E_{a,abstraction}$ given here, and the description of the addition channels, the parameters for which are given in Table 5.

	OH + F	OH + 2-MF	OH + 2,5-DMF
A_0 / cm^6 s^{-1}	6.6×10^{-22}	4.5×10^{-21}	3.1×10^{-20}
n	-9.50	-12.48	-11.76
A_∞ / cm^3 s^{-1}	2.9×10^{-11}	$5.7 \times ^{-11}$	8.93×10^{-11}
m	-1.05	-1.60	-1.85
x_0	1.041	0.707	0.541
b	0.427	0.254	0.323
F_{cent}	0.0187	0.066	0.125
$\Delta H^\ominus$ / kJ mol^{-1}	-159.3	-182.6	-165.0
$\Delta S^\ominus$ / J K^{-1} mol^{-1}	-100.2	-123.4	-79.5
Branching	1	$0.32\times(T/300)^{-0.24}$	1

Table 5: Troe fit parameters (Equations 1-6) to MESMER simulations for the addition channels for R1-R3 performed over the range 10^{15}-10^{21} cm^{-3} and 300-1300 K using the MESMER parameters determined from fitting to the experimental data. The thermodynamic parameters $\Delta H^\ominus$ and $\Delta S^\ominus$ are given for standard conditions (p = 1 bar). The overall rate coefficient for R1, R2, or R3 for a given pressure and temperature is given by the sum of the addition channels, the parameters for which are given here, and the abstraction rate coefficient described by the Arrhenius parameters $A_{abstraction}$ and $E_{a,abstraction}$ given in Table 4. For OH + 2-MF, the branching ratio describing the competition between addition to the C5 and C2 sites is also given, defined as the ratio of addition to the C2 position to that at C5 position.

Figures

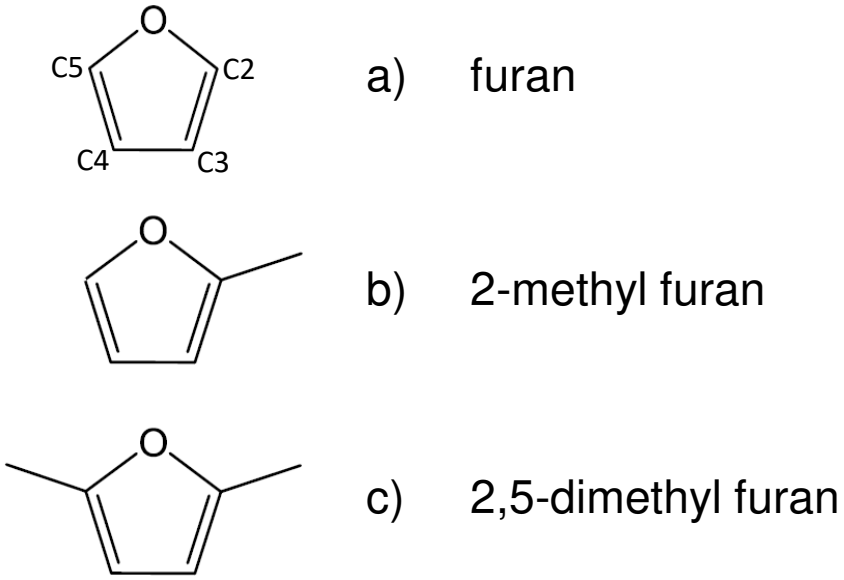

Figure 1: Molecular structures of a) furan (F), b) 2-methyl furan (2-MF), and c) 2,5-dimethyl furan (2,5-DMF). Labelled C atoms are shown for furan, and are equivalent for 2-methyl furan and 2,5-dimethyl furan.

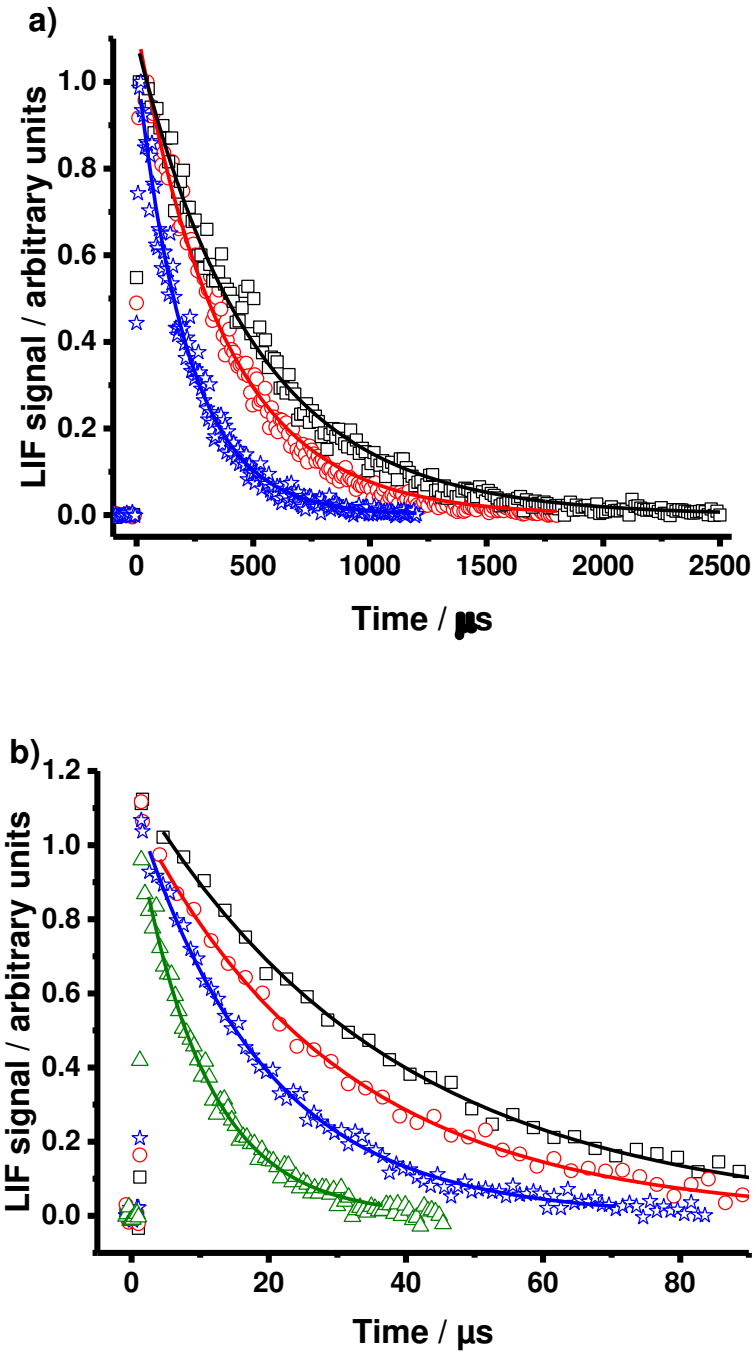

Figure 2: Typical OH profiles obtained for experiments at a) $p \leq 200$ mbar and b) $p \geq 2$ bar. Data shown for a) were obtained for OH + furan (R1) at $p = 67$ mbar, $T = 298$ K, and [furan] = 5.39×10^{13} cm^{-3} (black squares), 9.31×10^{13} cm^{-3} (red circles), and 1.33×10^{14} cm^{-3} (blue stars), with the corresponding fits (solid lines). Data shown for b) were obtained for OH + 2,5-dimethyl furan (R3) at $p = 5$ bar, $T = 380$ K, and [2,5-dimethyl furan] = 3.38×10^{14} cm^{-3} (black squares), 5.07×10^{14} cm^{-3} (red circles), 8.45×10^{14} cm^{-3} (blue stars), 1.68×10^{15} cm^{-3} (green triangles), with the corresponding fits (solid lines).

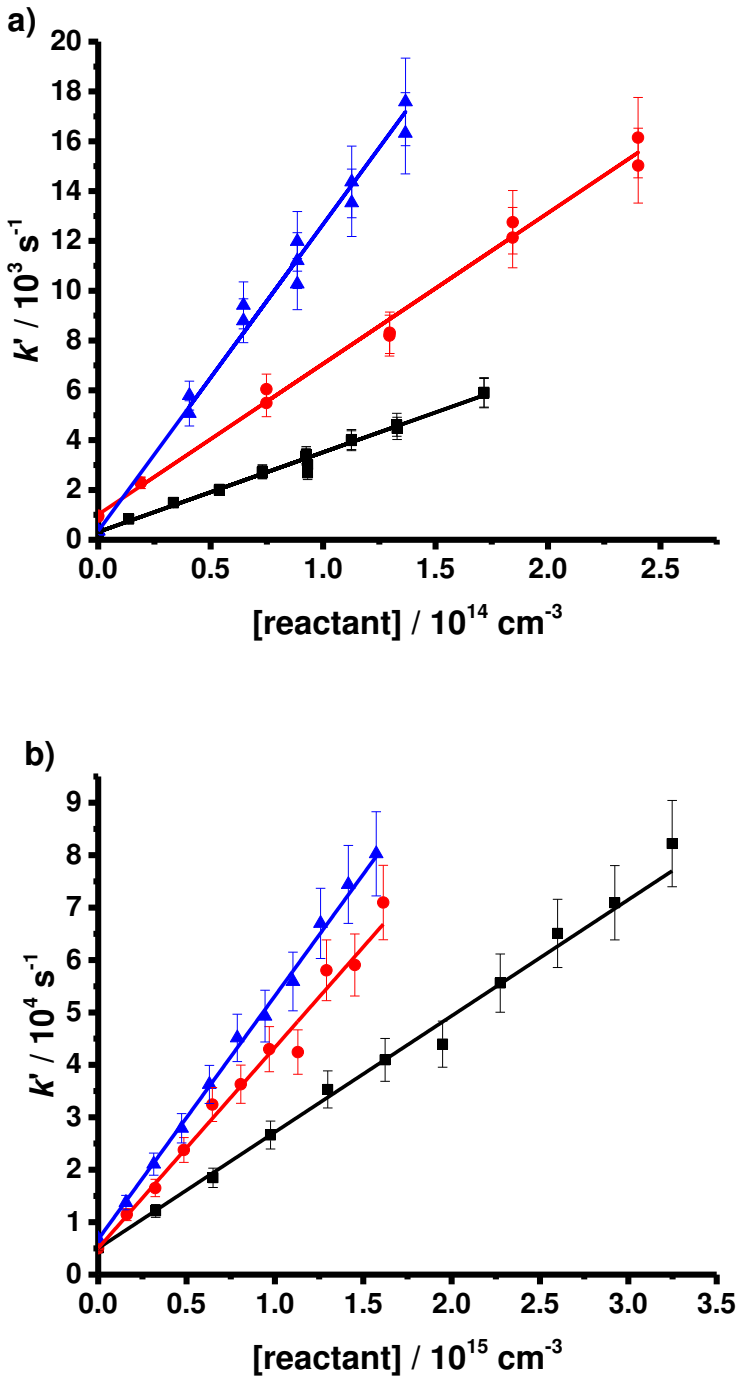

Figure 3: Typical bimolecular plots of the pseudo-first-order rate coefficients (k') obtained from fitting to OH profiles, as a function of the reactant concentration for experiments at a) $p \leq 200$ mbar and b) $p \geq 2$ bar. Data shown for a) were obtained for OH + furan (R1) at $p = 67$ mbar and $T = 298$ K (black squares), OH + 2-methyl furan (R2) at $p = 67$ mbar and $T = 340$ K (red circles), and OH + 2,5-dimethyl furan (R3) at $p = 67$ mbar and $T = 298$ K (blue triangles), with the corresponding fits (solid lines). Data shown for b) were obtained for OH + furan (R1) (black squares), OH + 2-methyl furan (R2) (grey diamonds) and OH + 2,5-dimethyl furan (R3) (light grey circles) at $p = 5$ bar and $T = 407$ K, with the corresponding fits (solid lines).

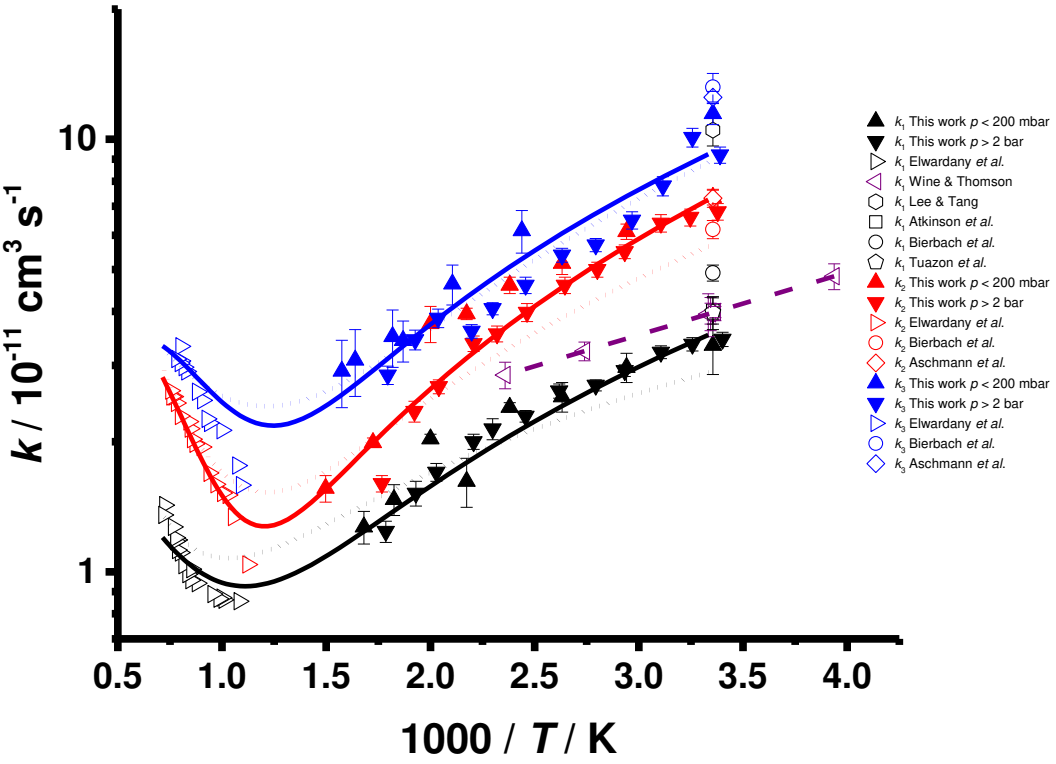

Figure 4: Effects of temperature on k_1 (black data points) k_2 (red data points) and k_3 (blue data points) obtained in this work for $p \leq 200$ mbar (filled up triangles) and $p \geq 2$ bar (filled down triangles). Results obtained in shock tube experiments by Elwardany *et al.*[25] (open right triangles), previous results for k_1 (open black data points), k_2 (open red data points), and k_3 (open blue data points) obtained at room temperature, and data obtained for k_1 by Wine and Thompson as a function of temperature (open purple left triangles and dashed line) are also shown. MESMER fits (solid lines) to the data are shown for k_1 (black), k_2, (red), and k_3 (blue). Troe fits (dotted lines) are also shown for k_1 (black), k_2, (red), and k_3 (blue) at a total pressure of 1.0 bar. Troe fits for total pressures of 0.5, 1.0 and 2 bar are generally indistinguishable from those at a total pressure of 1 bar.

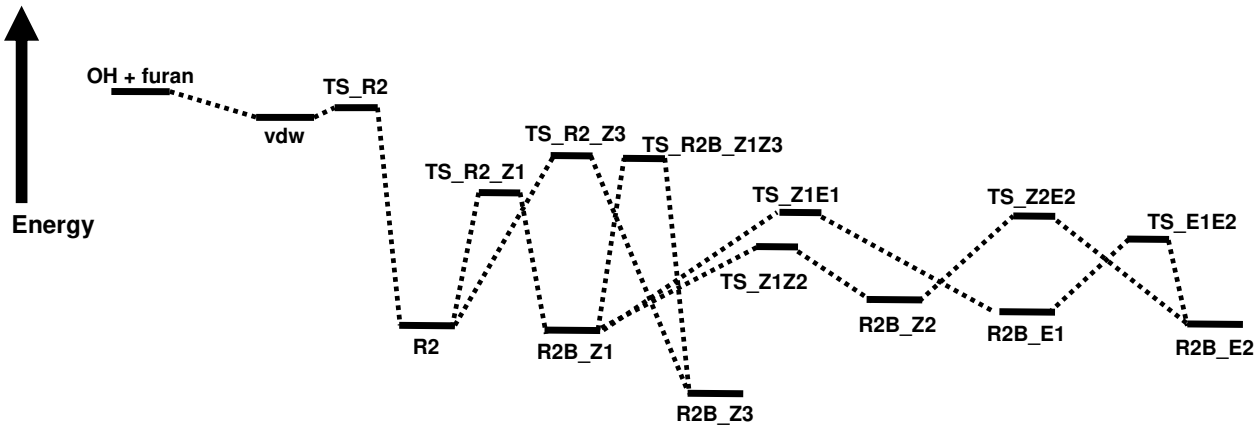

Figure 5: Potential energy surface for the initial steps in OH + furan reactions in the absence of O_2. Reproduced from the work of Yuan *et al.*[29], names of intermediates and transition states are those given by Yuan *et al*. The species R2 refers to addition at the 2-position of the furan ring. Details of structures are given in the Supporting Information. For reaction R1, the species R2B_Z3 is -179.9 kJ mol^{-1} below the entrance channel, for reaction R2 species R2B_Z3 is -185.1 kJ mol^{-1} below the entrance channel, and for reaction R3 species R2B_Z3 is -191.6 kJ mol^{-1} below the entrance channel at the RHF-UCCSD(T)-F12a/cc-pVDZ-F12 level of theory (including zero-point corrections).

References

1. Roman-Leshkov, Y.; Barrett, C. J.; Liu, Z. Y.; Dumesic, J. A. Production of Dimethylfuran for Liquid Fuels from Biomass-derived Carbohydrates. *Nature* **2007,** *447*, 982-985.
2. Wang, J. J.; Liu, X. H.; Hu, B. C.; Lu, G. Z.; Wang, Y. Q. Efficient Catalytic Conversion of Lignocellulosic Biomass into Renewable Liquid Biofuels via Furan Derivatives. *RSC Adv.* **2014,** *4*, 31101-31107.
3. Tong, X. L.; Ma, Y.; Li, Y. D. Biomass into Chemicals: Conversion of Sugars to Furan Derivatives by Catalytic Processes. *App. Cat. A* **2010,** *385*, 1-13.
4. Binder, J. B.; Raines, R. T. Simple Chemical Transformation of Lignocellulosic Biomass into Furans for Fuels and Chemicals. *J. Am. Chem. Soc.* **2009,** *131*, 1979-1985.
5. Eldeeb, M. A.; Akih-Kumgeh, B. Recent Trends in the Production, Combustion and Modeling of Furan-Based Fuels. *Energies* **2018,** *11,* 1-47.
6. Xu, N.; Gong, J.; Huang, Z. H. Review on the Production Methods and Fundamental Combustion Characteristics of Furan Derivatives. *Renew. Sust. Energ. Rev.* **2016,** *54*, 1189-1211.
7. Qian, Y.; Zhu, L. F.; Wang, Y.; Lu, X. C. Recent Progress in the Development of Biofuel 2,5-Dimethylfuran. *Renew. Sust. Energ. Rev.* **2015,** *41*, 633-646.
8. Liu, D.; Togbe, C.; Tran, L. S.; Felsmann, D.; Osswald, P.; Nau, P.; Koppmann, J.; Lackner, A.; Glaude, P. A.; Sirjean, B., *et al*. Combustion Chemistry and Flame Structure of Furan Group Biofuels using Molecular-Beam Mass Spectrometry and Gas Chromatography - Part I: Furan. *Combust. Flame* **2014,** *161*, 748-765.
9. Tran, L. S.; Togbe, C.; Liu, D.; Felsmann, D.; Osswald, P.; Glaude, P. A.; Fournet, R.; Sirjean, B.; Battin-Leclerc, F.; Kohse-Hoinghaus, K. Combustion Chemistry and Flame Structure of Furan Group Biofuels using Molecular-Beam Mass Spectrometry and Gas Chromatography - Part II: 2-Methylfuran. *Combust. Flame* **2014,** *161*, 766-779.
10. Togbe, C.; Tran, L. S.; Liu, D.; Felsmann, D.; Osswald, P.; Glaude, P. A.; Sirjean, B.; Fournet, R.; Battin-Leclerc, F.; Kohse-Hoinghaus, K. Combustion Chemistry and Flame Structure of Furan Group Biofuels using Molecular-Beam Mass Spectrometry and Gas Chromatography - Part III: 2,5-Dimethylfuran. *Combust. Flame* **2014,** *161*, 780-797.
11. Stockwell, C. E.; Jayarathne, T.; Cochrane, M. A.; Ryan, K. C.; Putra, E. I.; Saharjo, B. H.; Nurhayati, A. D.; Albar, I.; Blake, D. R.; Simpson, I. J., *et al*. Field Measurements of Trace Gases and Aerosols Emitted by Peat Fires in Central Kalimantan, Indonesia, During the 2015 El Nino. *Atmos. Chem. Phys.* **2016,** *16*, 11711-11732.
12. Muller, M.; Anderson, B. E.; Beyersdorf, A. J.; Crawford, J. H.; Diskin, G. S.; Eichler, P.; Fried, A.; Keutsch, F. N.; Mikoviny, T.; Thornhill, K. L., *et al*. In Situ Measurements and Modeling of Reactive Trace Gases in a Small Biomass Burning Plume. *Atmos. Chem. Phys.* **2016,** *16*, 3813-3824.
13. Hatch, L. E.; Yokelson, R. J.; Stockwell, C. E.; Veres, P. R.; Simpson, I. J.; Blake, D. R.; Orlando, J. J.; Barsanti, K. C. Multi-Instrument Comparison and Compilation of Non-Methane Organic Gas Emissions from Biomass Burning and Implications for Smoke-Derived Secondary Organic Aerosol Precursors. *Atmos. Chem. Phys.* **2017,** *17*, 1471-1489.
14. Koss, A. R.; Sekimoto, K.; Gilman, J. B.; Selimovic, V.; Coggon, M. M.; Zarzana, K. J.; Yuan, B.; Lerner, B. M.; Brown, S. S.; Jimenez, J. L., *et al*. Non-Methane Organic Gas Emissions from Biomass Burning: Identification, Quantification, and Emission Factors from PTR-ToF During the FIREX 2016 Laboratory Experiment. *Atmos. Chem. Phys.* **2018,** *18*, 3299-3319.
15. Ruzickova, J.; Kucbel, M.; Raclavska, H.; Svedova, B.; Raclavsky, K.; Juchelkova, D. Comparison of Organic Compounds in Char and Soot from the Combustion of Biomass in Boilers of Various Emission Classes. *J. Environ. Managet* **2019,** *236*, 769-783.
16. Majdi, M.; Sartelet, K.; Lanzafame, G. M.; Couvidat, F.; Kim, Y.; Chrit, M.; Turquety, S. Precursors and Formation of Secondary Organic Aerosols from Wildfires in the Euro-Mediterranean Region. *Atmos. Chem. Phys.* **2019,** *19*, 5543-5569.

17. Coggon, M. M.; Lim, C. Y.; Koss, A. R.; Sekimoto, K.; Yuan, B.; Gilman, J. B.; Hagan, D. H.; Selimovic, V.; Zarzana, K. J.; Brown, S. S., *et al*. OH Chemistry of Non-Methane Organic Gases (NMOGs) Emitted from Laboratory and Ambient Biomass Burning Smoke: Evaluating the Influence of Furans and Oxygenated Aromatics on Ozone and Secondary NMOG Formation. *Atmos. Chem. Phys.* **2019,** *19*, 14875-14899.
18. Sprengnether, M.; Demerjian, K. L.; Donahue, N. M.; Anderson, J. G. Product Analysis of the OH Oxidation of Isoprene and 1,3-Butadiene in the Presence of NO. *J. Geophys. Res. Atmos.* **2002,** *107*, 1-13.
19. Francisco-Marquez, M.; Alvarez-Idaboy, J. R.; Galano, A.; Vivier-Bunge, A. A Possible Mechanism for Furan Formation in the Tropospheric Oxidation of Dienes. *Environ. Sci. Tech.* **2005,** *39*, 8797-8802.
20. Lee, J. H.; Tang, I. N. Absolute Rate Constants for the Hydroxyl Radical Reactions with Ethane, Furan, and Thiophene at Room Temperature. *J. Chem. Phys.* **1982,** *77*, 4459-4463.
21. Atkinson, R.; Aschmann, S. M.; Carter, W. P. L. Kinetics of the Reactions of O_3 and OH Radicals with Furan and Thiophene at 298 ± 2 K. *Int. J. Chem. Kinet.* **1983,** *15*, 51-61.
22. Bierbach, A.; Barnes, I.; Becker, K. H. Rate Coefficients for the Gas-Phase Reactions of Hydroxyl Radicals with Furan, 2-Methylfuran, 2-Ethylfuran and 2,5-Dimethylfuran at 300 ± 2 K. *Atmos. Environ.* **1992,** *26*, 813-817.
23. Tuazon, E. C.; Atkinson, R.; Winer, A. M.; Pitts, J. N. A Study of the Atmospheric Reactions of 1,3-Dichloropropene and Other Selected Organochlorine Compounds. *Arch. Environ. Con. Tox.* **1984,** *13*, 691-700.
24. Aschmann, S. M.; Nishino, N.; Arey, J.; Atkinson, R. Kinetics of the Reactions of OH Radicals with 2- and 3-Methylfuran, 2,3- and 2,5-Dimethylfuran, and *E*- and *Z*-3-Hexene-2,5-dione, and Products of OH + 2,5-Dimethylfuran. *Environ. Sci. Tech.* **2011,** *45*, 1859-1865.
25. Elwardany, A.; Es-Sebbar, E.; Khaled, F.; Farooq, A. A Chemical Kinetic Study of the Reaction of Hydroxyl with Furans. *Fuel* **2016,** *166*, 245-252.
26. Wine, P. H.; Thompson, R. J. Kinetics of OH Reactions with Furan, Thiophene, and Tetrahydrothiophene. *Int. J. Chem. Kinet.* **1984,** *16*, 867-878.
27. Anglada, J. M. The Gas Phase HO-Initiated Oxidation of Furan: A Theoretical Investigation on the Reaction Mechanism. *Open Chem. Phys. J.* **2008,** *1*, 80-93.
28. Mousavipour, S. H.; Ramazani, S.; Shahkolahi, Z. Multichannel RRKM-TST and Direct-Dynamics VTST Study of the Reaction of Hydroxyl Radical with Furan. *J. Phys. Chem. A* **2009,** *113*, 2838-2846.
29. Yuan, Y.; Zhao, X. C.; Wang, S. N.; Wang, L. M. Atmospheric Oxidation of Furan and Methyl-Substituted Furans Initiated by Hydroxyl Radicals. *J. Phys. Chem. A* **2017,** *121*, 9306-9319.
30. Zhang, W. C.; Du, B. N.; Mu, L. L.; Feng, C. J. Computational Study on the Mechanism for the Reaction of OH with 2-Methylfuran. *J. Mol. Struc. Theochem.* **2008,** *851*, 353-357.
31. Davis, A. C.; Sarathy, S. M. Computational Study of the Combustion and Atmospheric Decomposition of 2-Methylfuran. *J. Phy. Chem. A* **2013,** *117*, 7670-7685.
32. Simmie, J. M.; Metcalfe, W. K. Ab Initio Study of the Decomposition of 2,5-Dimethylfuran. *J. Phys. Chem. A* **2011,** *115*, 8877-8888.
33. Whelan, C. A.; Blitz, M. A.; Shannon, R.; Onel, L.; Lockhart, J. P.; Seakins, P. W.; Stone, D. Temperature and Pressure Dependent Kinetics of QOOH Decomposition and Reaction with O_2: Experimental and Theoretical Investigations of QOOH Radicals Derived from Cl + $(CH_3)_3COOH$. *J. Phys. Chem. A* **2019,** *123*, 10254-10262.
34. Lockhart, J.; Blitz, M.; Heard, D.; Seakins, P.; Shannon, R. Kinetic Study of the OH plus Glyoxal Reaction: Experimental Evidence and Quantification of Direct OH Recycling. *J. Phys. Chem. A* **2013,** *117*, 11027-11037.
35. Carr, S. A.; Still, T. J.; Blitz, M. A.; Eskola, A. J.; Pilling, M. J.; Seakins, P. W.; Shannon, R. J.; Wang, B.; Robertson, S. H. Experimental and Theoretical Study of the Kinetics and Mechanism of the Reaction of OH Radicals with Dimethyl Ether. *J. Phys. Chem. A* **2013,** *117*, 11142-11154.

36. Bänsch, C.; Kiecherer, J.; Szöri, M.; Olzmann, M. Reaction of Dimethyl Ether with Hydroxyl Radicals: Kinetic Isotope Effect and Prereactive Complex Formation. *J. Phys. Chem. A* **2013,** *117*, 8343-8351.
37. Bänsch, C.; Olzmann, M. Reaction of Dimethoxymethane with Hydroxyl Radicals: An Experimental Kinetic Study at Temperatures Above 296 K and Pressures of 2, 5, and 10 bar. *Chem. Phys. Lett.* **2019,** *720*, 19-24.
38. Atkinson, R.; Baulch, D. L.; Cox, R. A.; Crowley, J. N.; Hampson, R. F.; Hynes, R. G.; Jenkin, M. E.; Rossi, M. J.; Troe, J. Evaluated Kinetic and Photochemical Data for Atmospheric Chemistry: Volume II - Gas Phase Reactions of Organic Species. *Atmos. Chem. Phys.* **2006,** *6*, 3625-4055.
39. Glowacki, D. R.; Liang, C. H.; Morley, C.; Pilling, M. J.; Robertson, S. H. MESMER: An Open-Source Master Equation Solver for Multi-Energy Well Reactions. *J. Phys. Chem. A* **2012,** *116*, 9545-9560.
40. Aschmann, S. M.; Nishino, N.; Arey, J.; Atkinson, R. Products of the OH Radical-Initiated Reactions of Furan, 2-and 3-Methylfuran, and 2,3-and 2,5-Dimethylfuran in the Presence of NO. *J. Phys. Chem. A* **2014,** *118*, 457-466.
41. Blitz, M. A.; Green, N. J. B.; Shannon, R. J.; Pilling, M. J.; Seakins, P. W.; Western, C. M.; Robertson, S. H. Reanalysis of Rate Data for the Reaction $CH_3 + CH_3 \rightarrow C_2H_6$ Using Revised Cross Sections and a Linearized Second-Order Master Equation. *J. Phys. Chem. A* **2015,** *119*, 7668-7682.
42. Medeiros, D. J.; Robertson, S. H.; Blitz, M. A.; Seakins, P. W. Direct Trace Fitting of Experimental Data Using the Master Equation: Testing Theory and Experiments on the $OH + C_2H_4$ Reaction. *J. Phys. Chem. A* **2020,** *124*, 4015-4024.
43. Medeiros, D. J.; Blitz, M. A.; James, L.; Speak, T. H.; Seakins, P. W. Kinetics of the Reaction of OH with Isoprene over a Wide Range of Temperature and Pressure Including Direct Observation of Equilibrium with the OH Adducts. *J. Phys. Chem. A* **2018,** *122* (37), 7239-7255.
44. Troe, J.; Ushakov, V. G. Representation of "Broad" Falloff Curves for Dissociation and Recombination Reactions. *Z. Phys. Chem.* **2014,** *228*, 1-10.

TOC Image

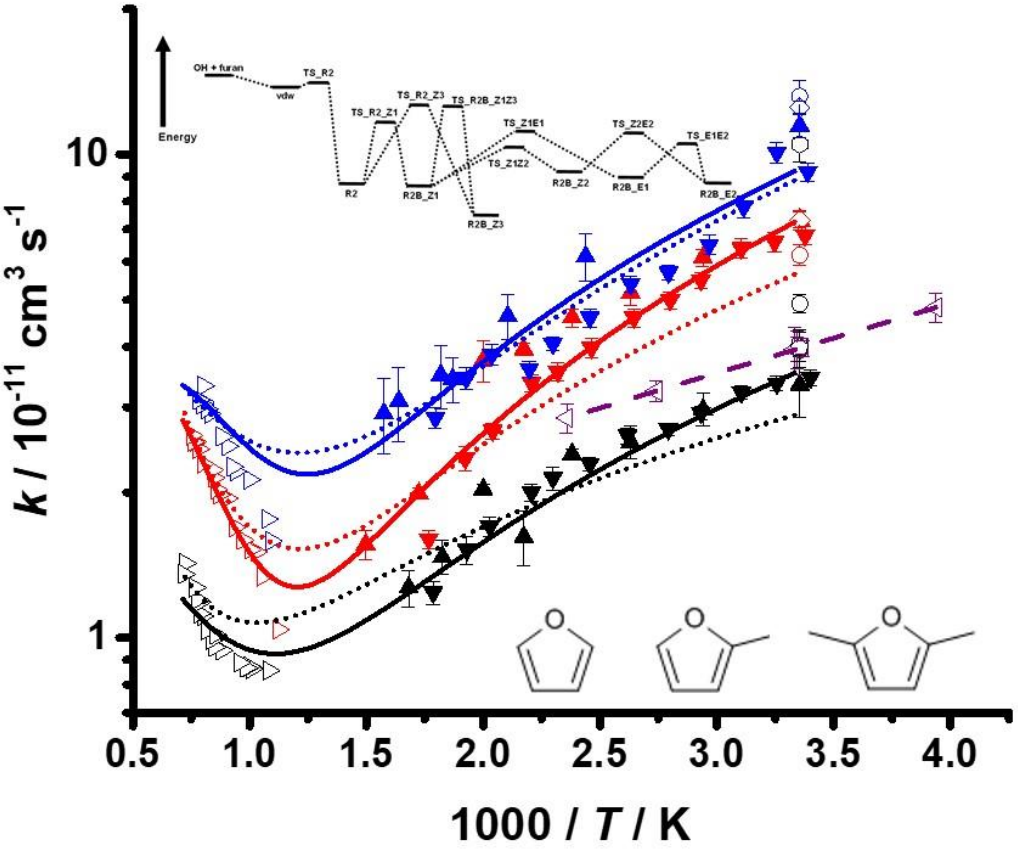
OH + furan
vdw
TS_R2
TS_R2_Z1
TS_R2_Z3
TS_R2B_Z1Z3
TS_Z1E1
TS_Z1Z2
TS_Z2E2
TS_E1E2
Energy
R2
R2B_Z1
R2B_Z3
R2B_Z2
R2B_E1
R2B_E2
10
1
k / 10-11 cm3 s-1
0.5
1.0
1.5
2.0
2.5
3.0
3.5
4.0
1000 / T / K